



THE UNIVERSITY
of ADELAIDE

The effect of solid particle recirculation on the efficiency of a cavity-type solar receiver

Md. Rabiul Islam Sarker

School of Mechanical Engineering

The University of Adelaide

South Australia 5005

Australia

**A dissertation submitted in fulfilment of the requirements for the
degree of Ph.D. in Engineering**

on the 12th March, 2015

PhD Thesis

Final version

12th March 2015

Thermo-fluid group

School of Mechanical Engineering

The University of Adelaide

South Australia 5005

Australia.

Typeset by the Author using MS Office 2010

Printed in Australia

Copyright © 2015, The University of Adelaide, South Australia

All right reserved. No part of this report may be used or reproduced in any form or by any means, or stored in a database or retrieval system without prior written permission of the university except in the case of brief quotations embodied in critical articles and reviews.

To my late parents

Abstract

High temperature steam or gas is used as the working medium for operation in advanced power conversion units, such as gas turbines or combined cycle power plants. The use of Concentrated Solar Power (CSP) technologies for energy generation relies on the heating of fluids to high temperatures. Conventional tubular or porous absorber volumetric receivers usually suffer from a relatively low thermal efficiency, less than 70%, and from high thermal losses. The solid particle solar receiver, in which the incoming solar radiation is directly absorbed by the solid particles and inner walls of the cavity receiver, promises to achieve higher thermal efficiency due to the enhanced heat transfer to the working fluid and the reduction in thermal losses. The main challenge in designing a high temperature solar receiver is to maximize the solar energy absorption and its efficient transfer to the working fluid, e.g. air. The objective of this research project is to characterize the thermal behaviour of a proposed cavity-type solar receiver concept based on the application of recirculating solid particles to achieve high temperature outlet air. In this concept, solar energy is absorbed by recirculating solid metallic particles, which, at the same time, transfer the absorbed thermal energy to the surrounding air in a cavity-type receiver. The cavity-type solid particle receiver is a well-insulated enclosure, designed to capture the incident solar radiation effectively, which allows the incident radiation directly through an aperture.

In this study, a well-insulated cavity-type enclosure was designed and constructed. The designed solar receiver consisted of an externally insulated cylindrical cavity with a circular aperture at the top covered by a quartz glass, a recirculating fan installed at the bottom of the chamber and with an inlet and an outlet installed on the chamber wall. A series of experiments were conducted to characterize the fluid dynamics and thermal behaviour of the solar receiver. The results showed that the direction of the total air flow velocity was vertically

upward from the outer periphery of the fan and vertically downward through the centre of the receiver. The measured air flow velocity was normalized by against the particle terminal velocity. The results showed that the normalized flow velocity was 3 times higher than the particles terminal velocity and 45 times higher than the minimum fluidization velocity of particles for the same case. Hence the particle can be recirculated in the cavity. The particles' concentration at different regions of the solar receiver was also measured using a laser-based light-scattering technique. Black SiC of 70micron and 200micron SiC particle were used during this experiment. The effect of particle size and fan RPM on the particle concentration at different regions of the solar receiver was optimized using the test results of the particle concentration measurements.

At an RPM of 1250, the measured opacity of the particle cloud's concentration was 0.95 for 70micron and 0.80 for 200micron particle at a specific freeboard height of the cavity. It is an indication that particles' concentration and opacity at a different region is dependent on the particle size and air flow velocity. The results showed that the particle concentration and opacity increased exponentially with the RPM. The opacity is a measure of the irradiation penetration characteristics of the Xenon arc radiation beam into the cavity.

The calculation of Stokes number and turbulence intensity from these measurements helped in understanding the slip velocity and velocity fluctuation of air and particles in the cavity. The maximum Stokes number was 0.50 for 70micron particle whereas it was 4 for 200 micron particle measured at 500RPM. Hence, when comparing the Stokes numbers it becomes clear that the slip velocity was higher for 200micron particles which denote more interaction with air. Turbulence intensity measurement showed that an average turbulence intensity of 38% was observed near the cavity wall and 30% at the centre of the cavity. Therefore, a better forced convection heat transfer was expected between the particle, air and cavity wall surface in the proposed receiver.

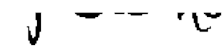
Finally a thermal test was performed to assess the thermal performance of the designed solar receiver. Black SiC and brown alumina particles at two sizes (70 and 200microns) were used in these experiments. The results showed that the air temperature in the solar receiver, when radiated by a 5kW Xenon arc lamp, increased by up to 83K resulting in a thermal efficiency of 55% for the proposed solar receiver. Here the air flow rate was set to 0.0055kg/s at an inlet temperature of 295K with no particles or fan forced circulation. When particles were added to the receiver, a 0.034% volume fraction, and the installed fan induced forced recirculation in the receiver the air temperature at the outlet of the receiver increased by 123K and the thermal efficiency reached 89% for the same air flow rate as before. The results of normalized thermal and power generation efficiency indicate that the use of recirculating particles enhances the thermal efficiency by 49% and power generation efficiency by 90%, when compared with the air only cavity-type solar receiver. Moreover the proposed recirculating flow receiver exhibits a more uniform temperature distribution than a conventional cavity-type solar receiver due to better mixing of air and particles, along with more effective radiation and convection heat transfer between them.

A stand-alone feature of this solar receiver concept is that the air with particles is directly exposed to concentrated solar radiation monotonously through the recirculating flow inside the receiver and results in an efficient irradiation absorption and convective heat transfer to the air. The increase of thermal and power generation efficiency of more than 50% proved that the developed concept has the potential to enhance heat transfer from metallic particles to air through maximizing the heat carrying capacity by the particles and air from the receiver.

Declaration of originality

This work contains no material that has been accepted for the award of any other degree or diploma in any university or other tertiary institution and, to the best of my knowledge and belief, contains no material previously published or written by another person, except where due reference has been made in the text. I give consent to this copy of my thesis, when deposited in the University Library, being made available for loan and photocopying, subject to the provisions of the Copyright Act 1968. I also give permission for the digital version of my thesis to be made available on the web, via the University's digital research repository, the Library catalogue, the Australasian Digital Theses Program (ADTP) and also through web search engines, unless permission has been granted by the University to restrict access for a period of time.

Signed:



(Md. Rabiul Islam Sarker)

Acknowledgement

With great thanks I acknowledge the generosity of many people that supported this research project. I would like to start by thanking Dr Maziar Arjomandi and Professor Bassam Dally for their support, advice and guidance throughout my PhD program. Their generous sharing of academic and practical expertise assisted me at all stages of my PhD process. I would like to thank the academic and general staff of the School of Mechanical Engineering for their help and support during my post graduate studies. In particular, Dr Zhiwei Sun, Dr Yunpeng Xue and Mr. Dahe Gu for their suggestions and help during the experiments, Mr Garry Clark, Mr. Richard Pateman, Mr. Steven Smith and Mr. Pascal Symons for technical assistance with the experimental rig construction and Mr. Billy Constantine for his help with information technology support. I would like to also thank all the friends that I have made in the School of Mechanical Engineering for their advice, assistance, comic relief, creative diversions and friendship over the years.

Special acknowledgment goes to Mr. Marc Simpson who spent considerable time assisting me with the solar simulator apparatus at the Mechanical Engineering Thebarton Research Laboratory, his technical support, interesting conversations and advice will always be remembered.

This work was financially supported by Commonwealth funding's from the Australian government and Commonwealth Science and Industrial research Organization (CSIRO). Special thanks go to Dr Sarah Millar who was the advisor from CSIRO under the Energy flagship scholarship. I would like to thank the Australian Government and CSIRO for their valuable financial support during this project.

Most importantly, I extend a million thanks to my family members, including my two children Ayesha and Joty, and especially to my wife Saeeda Akther, and father in law Mirza Md Naofel Uddin and mother in law Siddika Begum. I could not have completed this work without your wonderful love and support during the course of this project. A special

thanks to my elder brothers for their love and affection throughout my study. This thesis is dedicated to my father Md Abdur Rahman Sarker and my mother Khodeza Begum who would have been very proud to see me complete this major milestone in my life.

Contents

Abstract	v
Acknowledgement	ix
Chapter 1	1
Introduction	1
1.1 Introduction.....	1
1.2 State of the art.....	3
1.3 Motivation.....	7
1.4 Project goal and scope.....	11
1.5 Thesis outline.....	12
Chapter 2	15
Background Literature	15
2.1 Introduction.....	15
2.2 Tubular receiver design	16
2.3 Volumetric receiver design.....	18
2.3.1 Open volumetric receivers	21
2.3.2 Closed volumetric receivers	22
2.4 Solid particle solar receiver	26
2.5 Heat transfer and heat transfer media.....	32
2.6 Effect of particle concentration, particle size and recirculation rate.....	33
2.7 Particle selection	35
2.8 Project aim and objectives	36
Chapter 3	39
Problem statement and concept development	39
3.1 Introduction.....	39
3.2 Cavity receiver with air	41

3.3 Cavity receiver with ceramic honeycomb /foam.....	42
3.4 Cavity receiver with air and particles.....	43
3.5 Synthesis of the models.....	45
3.6 Recirculating flow solid particle solar receiver.....	55
3.7 Summary.....	57
Chapter 4.....	59
Experimental setup and Methodology	59
4.1 Introduction.....	59
4.2 Experimental investigations.....	59
4.3 SPSR design.....	60
4.3.1 Receiver material.....	61
4.3.2 Quartz window	62
4.3.3 Receiver sizing and geometry	63
4.3.4 Ducted axial flow fan	67
4.4 Air flow measurement	68
4.5 Particle concentration measurement	69
4.5.1 Experimental setup for particle concentration measurement	70
4.6 Experimental setup for thermal efficiency measurement.....	72
4.6.1 Temperature measurement.....	74
4.6.2 Solar simulator apparatus	75
4.6.3 Xenon short arc radiation source	76
4.6.4 Beam deflection mirror.....	79
4.7 Heat flux of a 5kW Xenon arc lamp.....	81
4.7.1 Heat flux measurement of the solar simulator.....	83
4.8 Summary.....	84

Chapter 5.....	87
Fluid dynamics behaviour	87
5.1 Introduction.....	87
5.2 Flow field measurement.....	87
5.2.1 Experimental procedure.....	88
5.2.2 Measurement uncertainties.....	91
5.2.3 Results and discussion	93
5.3 Particle concentration measurement.....	104
5.3.1 Experimental procedure.....	104
5.3.2 Measurement uncerainities	106
5.3.3 Results and discussion	106
5.3.4 Discussion on key findings	114
Chapter 6.....	119
Thermal behaviour analysis.....	119
6.1 Introduction.....	119
6.2 Heat flux measurement procedure	119
6.2.1 Measurement uncerainities	121
6.2.2 Results and discussion	122
6.3 Thermal behaviour of the receiver.....	125
6.3.1 Experimental procedure.....	125
6.3.2 Measurement uncertainties.....	126
6.3.4 Discussion on key findings	142
Chapter 7.....	151
Conclusions and Future study	151
7.1 Introduction.....	151
7.2 Conclusions	151
7.3 Recommendations for future research	153

References..... 155

List of Figures

FIGURE 1.1 CONCENTRATED SOLAR POWER (CSP) OFFERS AN INTEGRATED SOLUTION TO ENVIRONMENTAL POLLUTION IN THE COMING DECADES.	2
FIGURE 1.2 WORLD SOLAR ENERGY MAP [8].	3
FIGURE 1.3 CURRENT LARGE SCALE CSP PROJECT GOAL [9, 10].....	4
FIGURE 1.4 CSP SYSTEMS INCLUDING (A) TROUGH SYSTEM (B) FRESNEL SYSTEM (C) DISH SYSTEM AND (D) TOWER SYSTEM [13].	5
FIGURE 1.5 CSP BASED SYSTEM OPERATING TEMPERATURE SCENARIO [14].....	5
FIGURE 1.6 A HYBRID SOLAR POWER TOWER PLANT.	7
FIGURE 1.7A EXTERNAL TYPE SOLID PARTICLE SOLAR RECEIVERS [11].	10
FIGURE 1.7B CAVITY TYPE (RIGHT) SOLID PARTICLE SOLAR RECEIVERS [11].	11
FIGURE 2.1 TUBULAR RECEIVER [30].	16
FIGURE 2.2 OPEN VOLUMETRIC HIT RECEIVER [11].....	18
FIGURE 2.3 CAVITY TYPE VOLUMETRIC RECEIVERS [37].	19
FIGURE 2.4 CERAMIC FOAM AS AN IRRADIATION ABSORBING MATERIAL USED IN A VOLUMETRIC RECEIVER [38, 39].....	19
FIGURE 2.5 SILICON CARBIDE FIBRE MESH, METALLIC AND SILICON CARBIDE CERAMIC CARRIER CATALYSTS [38, 39].	20
FIGURE 2.6 DIRECT ABSORPTION CAVITY TYPE SOLAR DIAPAR RECEIVER [49].....	24
FIGURE 2.7 CONCEPTUAL DESIGN OF SMALL CARBON PARTICLE SOLAR RECEIVER [55].	28
FIGURE 2.8 A CONCEPTUAL DESIGN OF A FREELY FALLING SOLID PARTICLE RECEIVER [55].....	30
FIGURE 2.9 SCHEMATIC OF A CAVITY TYPE, DIRECT ABSORPTION, VORTEX FLOW SOLAR CHEMICAL REACTOR [20, 62].	30
FIGURE 2.10 CONCEPTUAL DESIGN OF AN INTERNALLY RECIRCULATING SOLAR CHEMICAL REACTOR [55].	31
FIGURE 2.11 (A) DIRECT AND (B) INDIRECT HEAT TRANSFER MODES IN A CSP RECEIVER.	32
FIGURE 3.1 SCHEMATIC OF THE CAVITY RECEIVER MODEL WITH DETAILS OF THE DIFFERENT HEAT TRANSFER MODES.	40
FIGURE 3.2 EFFECT OF THE PARTICLE VOLUME FRACTION ON CONVECTION HEAT TRANSFER COEFFICIENTS BETWEEN THE PARTICLES AND AIR.	45

FIGURE 3.3 VARIATION OF (A) OUTLET AIR TEMPERATURE (B) THERMAL EFFICIENCY WITH THE MASS FLOW RATE OF AIR INTO A CAVITY TYPE SOLAR RECEIVER	47
FIGURE 3.4 SCHEMATIC OF A CAVITY TYPE SOLAR RECEIVER MODEL.	50
FIGURE 3.5 CAVITY TEMPERATURE DISTRIBUTION OF A CAVITY TYPE SOLAR RECEIVER (A) NATURAL CONVECTION WITH AIR (B) FORCED CONVECTION WITH AIR (C) FORCED CONVECTION WITH AIR AND PARTICLE MIXTURE.	52
FIGURE 3.6 VARIATION OF OUTLET AIR TEMPERATURE WITH THE MASS FLOWRATE OF AIR IN THE SOLAR RECEIVER	53
FIGURE 3.7 VARIATION OF THERMAL EFFICIENCY USING AIR ONLY AND AIR WITH PARTICLES INTO THE RECIRCULATING FLOW SOLAR RECEIVER	55
FIGURE 3.8 DIMENSIONLESS THERMAL EFFICIENCY AND OUTLET AIR TEMPERATURE AS A FUNCTION OF MASS FLOWRATE OF THE INJECTED AIR.	55
FIGURE 3.9 RECIRCULATING FLOW SOLID PARTICLE SOLAR RECEIVER.	57
FIGURE 4.1 TRANSMITTANCE CHARACTERISTICS OF FUSED QUARTZ GLASS [98].	63
FIGURE 4.2 ASSEMBLY OF THE DESIGNED RECEIVER AND A PHOTOGRAPH OF THE MANUFACTURED RECEIVER.	66
FIGURE 4.3 SCHEMATIC OF THE DESIGNED JET PASSAGE SURROUNDING THE APERTURE.	67
FIGURE 4.4 SCHEMATIC OF AIR FLOWING MEASUREMENT SETUP.	68
FIGURE 4.5 PHOTOGRAPHIC VIEW OF ALIGNMENT TEST OF THE COBRA PROBE.	68
FIGURE 4.6 SCHEMATIC OF THE OPTICS AND CALIBRATION CELL FOR THE PARTICLES' ATTENUATION TEST AT DIFFERENT CONCENTRATIONS OF WATER/PARTICLE MIXTURES.	71
FIGURE 4.7 SCHEMATIC OF THE LASER OPTICS WITH THE SOLAR RECEIVER FOR PARTICLES' CONCENTRATION MEASUREMENT.	71
FIGURE 4.8 SCHEMATIC OF EXPERIMENTAL DESIGN FOR THERMAL TESTING OF THE SOLAR RECEIVER.	74
FIGURE 4.9 SCHEMATIC OF THE SOLAR SIMULATOR APPARATUS [100].	77
FIGURE 4.10 PHOTOGRAPH OF THE HLR OSRAM 5kW XENON SHORT-ARC LAMP USED IN THE EXPERIMENT.	78
FIGURE 4.11 SPECTRAL INTENSITY OF A XENON ARC LAMP COMPARED WITH EXTRA-TERRESTRIAL AND GROUND LEVEL SOLAR IRRADIANCE [100]	78
FIGURE 4.12 CALCULATED BEAM DIAMETER, D_B AS A FUNCTION OF DISTANCE FROM THE REAR OF THE LAMP HOUSING'S REFLECTOR [103].	80

FIGURE 4.13 REFLECTANCE OF STAINLESS STEEL, ALUMINIUM AND SILVER BETWEEN 0.3 μ M AND 2.5 μ M [102].	81
FIGURE 4.14 CALCULATED BEAM DIAMETER D_B AND AVERAGE HEAT FLUX Q_{ELEC} , AS A FUNCTION OF DISTANCE S FROM THE FOCAL POINT FOR 49% CONVERSION EFFICIENCY.....	83
FIGURE 4.15 SCHEMATIC OF EXPERIMENTAL SETUP FOR THE HEAT FLUX MEASUREMENT OF THE XENON ARC SOLAR SIMULATOR.	84
FIGURE 5.1 SCHEMATIC AND PHOTOGRAPHIC VIEW OF THE VELOCITY MEASUREMENT SETUP.	88
FIGURE 5.2 SCHEMATIC CROSS SECTION VIEWS SHOWING AIR FLOW MEASUREMENT LOCATIONS (RECEIVER WITH DUCTED FAN) AND GEOMETRICAL ARRANGEMENT (A) XY CROSS SECTION (B) XZ CROSS SECTION.	90
FIGURE 5.3 SCHEMATIC OF THE CROSS SECTION VIEWS OF THE RECEIVER CYLINDRICAL PART SHOWING STOPPER LOCATION (RECEIVER WITH PARTICLE STOPPER).....	91
FIGURE 5.4 PHOTOGRAPH OF TESTING THE QUARTZ WINDOW WITH RECIRCULATING PARTICLES AT 1500RPM (WITH AIR JET AND PARTICLE STOPPER).....	91
FIGURE 5.5 VARIATION OF COBRA PROBE ACCURACY WITH RESPECT TO PITOT- STATIC PROBE.....	93
FIGURE 5.6 VARIATION OF TOTAL FLOW VELOCITY WITH THE RADIAL POSITION ALONG THE X AXIS AT $Z=\pm 180$ MM AND RPM=1500.....	95
FIGURE 5.7 VARIATION OF TOTAL FLOW VELOCITY OF AIR WITH THE RADIAL POSITION ALONG THE X AXIS AT $Z=\pm 30$ MM AT RPM=1500.....	96
FIGURE 5.8 VARIATION OF AXIAL FLOW VELOCITY OF AIR WITH THE RADIAL POSITION ALONG THE X AXIS AT $Z=\pm 180$ MM AT RPM 1500.....	97
FIGURE 5.9 VARIATION OF TOTAL FLOW VELOCITY AND AXIAL FLOW VELOCITY WITH THE RADIAL POSITION ALONG THE X AXIS AT $Y=350$ MM (RPM=1500).	99
FIGURE 5.10 VARIATION OF TOTAL FLOW VELOCITY AXIAL FLOW VELOCITY WITH THE RADIAL POSITION ALONG THE X AXIS AT $Y=350$ MM (RPM=800).....	99
FIGURE 5.11 VARIATION OF TOTAL FLOW VELOCITY AXIAL FLOW VELOCITY WITH THE RADIAL POSITION ALONG THE X AXIS AT $Y=350$ MM (RPM=500).....	100
FIGURE 5.12 VARIATION OF TANGENTIAL VELOCITY WITH THE RADIAL POSITION ALONG THE X AXIS AT (A) $Z=+30$ MM AND (B) $Z=+180$ MM (RPM=800).	100

FIGURE 5.13 VARIATION OF NORMALIZED (A) TERMINAL VELOCITY (B) MINIMUM FLUIDIZATION VELOCITY WITH THE RADIAL POSITION ALONG THE X AXIS AT $Z=\pm 180\text{MM}$, RPM=500. FIGURE 5.14 VARIATIONS OF TURBULENCE INTENSITY WITH THE RADIAL POSITION ALONG THE X AXIS AT $Z=+180\text{MM}$ AT 1500RPM. 102	102
FIGURE 5.15 VARIATION OF TURBULENCE INTENSITY WITH THE RADIAL POSITION ALONG THE X AXIS AT 800RPM.	103
FIGURE 5.16 VARIATIONS IN TURBULENCE INTENSITY WITH THE RADIAL POSITION ALONG THE X AXIS AT 500RPM.	103
FIGURE 5.17 SCHEMATIC AND PHOTOGRAPH OF THE PARTICLE CONCENTRATION MEASUREMENT EXPERIMENTAL SETUP (SCHEMATIC SHOWN IN FIGURE 4.7). ...	105
FIGURE 5.18 CALIBRATION CURVE FOR (A) 70 MICRON AND (B) 200MICRON PARTICLES.	107
FIGURE 5.19 MEASURED PARTICLE CONCENTRATION FOR 70 AND 200MICRON SiC PARTICLES AT DIFFERENT FAN SPEED AND AT A FREE BOARD HEIGHT OF (A) $Y=430\text{MM}$, (B) $Y=590\text{MM}$, AND (C) $Y=840\text{MM}$	108
FIGURE 5.20 MEASURED PARTICLE CONCENTRATION FOR 200MICRON SiC PARTICLES AT DIFFERENT FAN SPEED AND AT DIFFERENT DIMENSIONLESS HEIGHTS.	111
FIGURE 5.21 MEASURED PARTICLE CONCENTRATION FOR 200MICRON SiC PARTICLE AT DIFFERENT DIMENSIONLESS HEIGHT AND AT A SPEED 1000RPM.	112
FIGURE 5.22 VARIATION OF OPACITY WITH CHANGING (A) FAN SPEED AT $Y=840\text{MM}$ AND (B) DIMENSIONLESS HEIGHT AT 1260RPM.	112
FIGURE 5.23 VARIATION OF THE STOKES NUMBERS WITH THE RADIAL POSITION OF THE SOLAR RECEIVER FOR (A) 200 AND (B) 70MICRONS SiC.	113
FIGURE 5.24 SCHEMATIC OF FLOW PATTERN (A) CURRENT RECIRCULATING FLOW SOLID PARTICLE SOLAR RECEIVER WITH FAN (B) SOLAR RECEIVER WITHOUT FAN	114
FIGURE 5.25 (A) EFFECT OF RPM ON THE CAVITY REYNOLDS NUMBER AND TURBULENCE INTENSITY (B) VARIATION OF STOKES NUMBER AND PARTICLE CONCENTRATION WITH THE CHANGE OF REYNOLDS NUMBER (C) VARIATION OF NORMALIZED FLOW VELOCITY WITH THE ROTATIONAL SPEED OF THE FAN.	117
FIGURE 6.1 HEAT FLUX MEASUREMENT SETUP WITH THE LOCATION OF MEASUREMENTS. $S_1=900\text{MM}$, $S_2=1000\text{MM}$, $S_3=1100\text{MM}$ AND $S_4=1200\text{MM}$...	120
FIGURE 6.2 HEAT FLUX MEASUREMENT GRID POINTS LOCATION ON XZ PLANE.	121

FIGURE 6.3 HEAT FLUX DISTRIBUTION USING ONLY THE BEAM DOWN MIRROR, WITH THE TARGET POINT AT A DISTANCE OF 20MM FROM THE FOCAL POINT; (A) $S_1=900\text{MM}$ (B) $S_2=1000\text{MM}$ (C) $S_3=1100\text{MM}$ (D) $S_4=1200\text{MM}$	123
FIGURE 6.4 HEAT FLUX DISTRIBUTION USING THE BEAM DOWN MIRROR AND QUARTZ GLASS ON THE APERTURE, THE BEAM TARGET POINT ON THE MIRROR AT A DISTANCE 20MM FROM THE FOCAL POINT; (A) $S_1=900\text{MM}$ (B) $S_2=1000\text{MM}$ (C) $S_3=1100\text{MM}$ (D) $S_4=1200\text{MM}$	124
FIGURE 6.5 SCHEMATIC AND PHOTOGRAPH OF THE THERMAL PERFORMANCE EXPERIMENTAL SETUP.	128
FIGURE 6.6 VARIATIONS OF AIR TEMPERATURE WITH CHANGING FAN SPEED AT A MASS FLOW RATE OF 0.0044KG/S; (A) VOLUME FRACTION=0.022% (B) VOLUME FRACTION=0.044%.....	130
FIGURE 6.7 PHOTOGRAPH OF QUARTZ WINDOW SHOWING PARTICLE DEPOSITION.	131
FIGURE 6.8 OUTLET AIR TEMPERATURE (T_a) VS FAN SPEED (N) AT DIFFERENT MASS FLOW RATES OF AIR AND DIFFERENT FREE BOARD HEIGHT OF THE RECEIVER; (A) $Y=300\text{MM}$, 200MICRON SiC (B) $Y=400\text{MM}$, 200MICRON SiC (C) $Y=400\text{MM}$, 200MICRON Al_2O_3 (D) $Y=500\text{MM}$, 200MICRON SiC.....	134
FIGURE 6.9 RECEIVER THERMAL EFFICIENCY VS AIR MASS FLOW RATE AT DIFFERENT FAN SPEEDS; (A) $Y=300\text{MM}$, 200MICRON SiC (B) $Y=400\text{MM}$, 200MICRON SiC (C) $Y=400\text{MM}$, 200MICRON Al_2O_3 (D) $Y=500\text{MM}$, 200MICRON SiC.....	137
FIGURE 6.10 CHANGE OF DIVERGING BEAM DIAMETERS AT A DISTANCE L (MM) AWAY THE FOCAL POINT.	137
FIGURE 6.11 POWER CONVERSION EFFICIENCY VS MASS FLOW RATES OF AIR AT DIFFERENT FAN SPEEDS; (A) $Y=300\text{MM}$, 200MICRON SiC (B) $Y=400\text{MM}$, 200MICRON SiC (C) $Y=400\text{MM}$, 200MICRON Al_2O_3 (D) $Y=500\text{MM}$, 200MICRON SiC.....	139
FIGURE 6.12 NORMALIZED THERMAL EFFICIENCY VS FAN SPEED AT DIFFERENT MASS FLOW RATES OF AIR; (A) $Y=300\text{MM}$, 200MICRON SiC (B) $Y=400\text{MM}$, 200MICRON SiC (C) $Y=400\text{MM}$, 200MICRON Al_2O_3 (D) $Y=500\text{MM}$, 200MICRON SiC.	140
FIGURE 6.13 NORMALIZED POWER CONVERSION EFFICIENCY VS FAN SPEED AT DIFFERENT MASS FLOW RATES OF AIR; (A) $Y=300\text{MM}$, 200MICRON SiC (B) $Y=400\text{MM}$, 200MICRON SiC (C) $Y=400\text{MM}$, 200MICRON Al_2O_3 (D) $Y=500\text{MM}$, 200MICRON SiC.	141
FIGURE 6.14 EFFECT OF (A) VOLUME FRACTION ON TEMPERATURE, THERMAL EFFICIENCY AND (B) HEAT TRANSFER COEFFICIENT BETWEEN PARTICLES AND AIR.	143
FIGURE 6.15 EFFECT OF (A) FAN SPEED ON CAVITY REYNOLDS NUMBER AND NUSSELT NUMBER (B) HEAT TRANSFER ENHANCEMENT WITH THE CAVITY REYNOLDS NUMBER.	143
FIGURE 6.16 VARIATION OF CAVITY WALL TEMPERATURE FOR DIFFERENT RPM AT AIR FLOW RATE OF 0.0055KG/SEC.	144

FIGURE 6.17 SIMULATED FLUID FLOW PATTERN WITH THE DUCT (LEFT) AND WITH THE STOPPER (RIGHT).	146
FIGURE 6.18 SCHEMATIC OF THE RECEIVER SHOWING BEAM PENETRATION,	149
FIGURE 6.19 VARIATION OF DIMENSIONLESS TEMPERATURE AND THERMAL EFFICIENCY WITH DIMENSIONLESS HEIGHT.	150

List of Tables

TABLE 2.1 PROPERTIES OF SiC AND Al_2O_3	36
TABLE 3.1 COMPARISON BETWEEN THE DIFFERENT TYPES OF SOLAR RECEIVERS [28].....	45
TABLE 4.1 PROPERTIES OF STAINLESS STEEL (SS316).....	62
TABLE 4.2 SPECIFICATION FOR THE XENON XBO 5000W/HBM OSRM LAMP.	77
TABLE 4.3 SOLAR ENERGY CONVERSION OF XENON LIGHT SOURCE.....	82
TABLE 4.4 SPECTRUM ANALYSIS OF XENON LAMP LIGHT SOURCE.	82
TABLE 4.5 HEAT FLUX TRANSDUCER SPECIFICATION.	83
TABLE 5.1 TABLE SHOWING THE MEASUREMENT LOCATIONS	94
TABLE 6.1 COMPARISON OF MEASURED HEAT FLUX USING THE MIRROR AND QUARTZ GLASS AT FOUR AXIAL DISTANCES FROM THE FOCAL POINT.....	123
TABLE 6.2 TEST CONDITIONS FOR AIR AS A HEAT TRANSFER MEDIUM.	127
TABLE 6.3 TEST CONDITIONS FOR AIR AND PARTICLES AS A HEAT TRANSFER MEDIUM.....	129
TABLE 6.4 SIZE ANALYSIS OF 70MICRON SiC PARTICLES [109].....	131
TABLE 6.5 SIZE ANALYSIS OF 200 MICRON SiC PARTICLES [109].	131

Nomenclature

η	Efficiency
α	Absorption coefficient
$Q_{aperture}$	Power at aperture
ε	Emissivity
$A_{aperture}$	Aperture area
T	Temperature
Q	Solar power (Watt)
C	Concentration ratio
$r_{aperture}$	Aperture radius
r_{opt}	Optimum aperture radius
μ	Standard deviation
F_{peak}	Maximum flux density
I	Scattered light Intensity
l	Reference path length of medium
λ	Wavelength
x	Particle size
n	Index of refraction
θ	Scattered angle
c	Particle concentration
v_t	Terminal velocity
v_t^*	Dimensionless terminal velocity
μ_g	Viscosity of gas
ρ	Density
g	Acceleration
d_p	Particle diameter
D	Receiver diameter
τ	Response time
Nu	Nusselt number
Re	Reynolds number
Pr	Prandtl number

St	Stokes number
h	Heat transfer coefficient
A	Cavity surface area
I_G	Incident irradiation
k_f	Thermal conductivity of fluid
U_0	Free stream velocity of fluid
α_{sf}	The porosity of the porous medium
α_p	Particle volume fraction
V_{rms}	Root mean square air velocity
V	Total velocity of air
V_y	Axial component of air velocity
V_θ	Tangential velocity component
V_t	Volume of the whole receiver
M	Suspended particle concentration in air
N	Rotational speed of fan
CSP	Concentrated Solar Power
CST	Concentrated Solar Thermal
SPSR	Solid Particle Solar Receiver
HTM	Heat transfer medium
HTF	Heat transfer fluid
CPC	Compound Parabolic Collector
PLVCR	Pressurized Loaded Volumetric Ceramic Receiver
DIAPR	Directly Irradiated Annular Pressurize Receiver
NREL	National Renewable Energy Laboratory
SNL	Sandia National Laboratory
DLR	German Aerospace Centre
CIEMAT	Organisation of Plataforma Solar de Almeria
CSIRO	The Commonwealth Scientific and Industrial Research Organisation , Australia

Suffix

a	air
c	cavity
g	gas
m	mixture

p	particle
τ	thermal
o	overall
a,in	inlet air
a,o	outlet air